

Thickness tunable Kerr nonlinearity in BiOBr nanoflakes

This paper was downloaded from TechRxiv (<https://www.techrxiv.org>).

LICENSE

CC BY 4.0

SUBMISSION DATE / POSTED DATE

23-08-2020 / 25-08-2020

CITATION

Moss, David (2020): Thickness tunable Kerr nonlinearity in BiOBr nanoflakes. TechRxiv. Preprint.
<https://doi.org/10.36227/techrxiv.12847091.v1>

DOI

[10.36227/techrxiv.12847091.v1](https://doi.org/10.36227/techrxiv.12847091.v1)

Thickness tunable Kerr nonlinearity in BiOBr nanoflakes

Linnan Jia^a, Dandan Cui^b, Jiayang Wu^a, Haifeng Feng^c, Tieshan Yang^d,
Yunyi Yang^d, Yi Du^c, Weichang Hao^b, Baohua Jia^{a,d}, David J. Moss^{a,*}

^aOptical Sciences Centre, Swinburne University of Technology, Hawthorn, VIC 3122, Australia

^bSchool of Physics, and BUAA-UOW Joint Research Centre, Beihang University, Beijing 100191, China

^cInstitute for Superconducting and Electronic Materials, and UOW-BUAA Joint Research Centre, University of Wollongong, Wollongong, NSW 2500, Australia

^dCentre for Translational Atomaterials, Swinburne University of Technology, Hawthorn, VIC 3122, Australia

*E-mail: dmoss@swin.edu.au

Abstract: We report a high Kerr optical nonlinearity in BiOBr nanoflakes that varies with thickness via the Z-Scan technique. We integrate BiOBr nanoflakes onto silicon integrated nanowires and characterize the linear optical properties of the hybrid integrated devices.

1. Introduction

Two-dimensional (2D) layered materials have attracted significant interest recently for their remarkable nonlinear optical properties such as strong nonlinear absorption [1 - 4], ultrafast broadband optical response [1, 2], and ultrahigh Kerr optical nonlinearity [3-6]. Amongst them, bismuth oxyhalides, i.e., BiOX (X = Cl, Br, I), which consist of $[\text{Bi}_2\text{O}_2]^{2+}$ slabs interleaved with double halogen atoms with weak van der Waals interaction between the adjacent halogen slabs, have been explored as a new group of advanced layered optical materials [7, 8]. The self-built internal static electric field resulting from asymmetric charge distribution between the $[\text{Bi}_2\text{O}_2]^{2+}$ and halogen layers in BiOX leads to an effective separation of photoinduced electro-hole pairs, which enables prominent photocatalytic properties [7, 8] as well as a high third-order nonlinear optical response [9].

In this work, we characterize the third-order optical nonlinearity of BiOBr nanoflakes—an important member of BiOX family—via Z-scan technique. Experimental results show that BiOBr exhibits a strong two photon absorption (TPA- β) of $\sim 10^{-7}$ m/W and a large Kerr coefficient n_2 of $\sim 10^{-14}$ m²/W at 800 nm wavelength. Moreover, the nonlinear optical response in BiOBr is shown to depend strongly on thickness, with the magnitude of β and n_2 increasing significantly for very thin flake thicknesses. We also integrate the BiOBr nanoflakes onto silicon integrated waveguides and measure the linear optical properties, with the waveguide propagation loss showing good agreement with mode simulations. Our results confirm the strong potential of BiOBr as an advanced nonlinear optical material for the implementation of high-performance nonlinear photonic devices.

2. Material preparation and characterization

BiOBr nanoflakes with different thicknesses were mechanically exfoliated from the bulk crystals onto glass substrates using adhesive tapes. Fig. 1(a) shows the thickness profiles of the prepared BiOBr nanoflakes. The measured thicknesses of the samples in (i) – (iv) are ~ 30 nm, ~ 75 nm, ~ 110 nm, and ~ 140 nm, respectively.

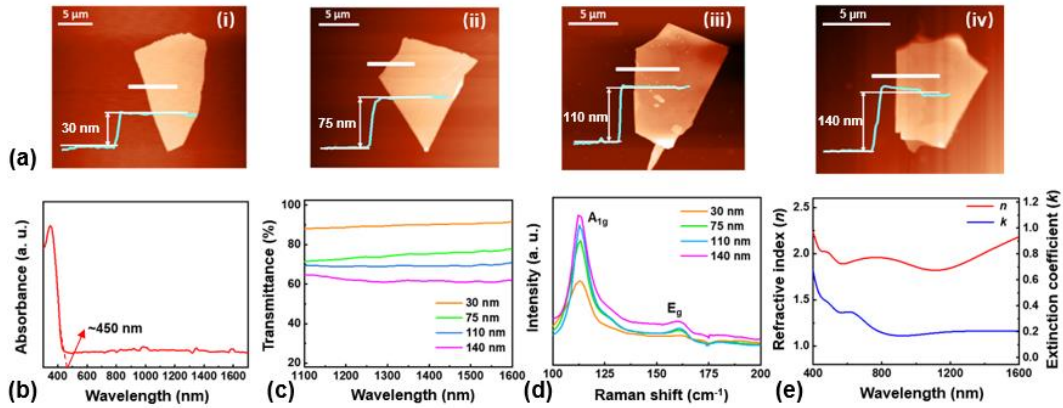


Fig. 1 (a) AFM thickness profiles of exfoliated BiOBr nanoflakes with various thicknesses: (i) ~ 30 nm, (ii) ~ 75 nm, (iii) ~ 110 nm, (iv) ~ 140 nm. (b) UV-vis absorption spectrum of BiOBr. (c) Measured linear transmittance spectra and (d) Raman spectra of BiOBr nanoflakes with different thicknesses. (e) Measured refractive index (n) and extinction coefficient (k) of BiOBr.

Fig. 1(b) depicts the linear absorption of BiOBr from 300 nm to 1700 nm measured by ultraviolet-visible (UV-vis) spectrometry. A clear absorption edge at ~ 450 nm is observed, which corresponds to a photon energy of ~ 2.76 eV, in agreement with the reported bandgap of BiOBr [7, 8]. The measured transmittance spectra of BiOBr nanoflakes with different thicknesses are also shown in Fig. 1(c). Fig. 1(d) shows the Raman spectra of BiOBr samples with an incident laser at 532 nm. Two typical phonon modes of A_{1g} (~ 113.2 cm⁻¹) and E_g (~ 160.4 cm⁻¹) are observed for all samples, verifying the high quality of the prepared BiOBr nanoflakes [7]. Fig. 1(e) shows the in-plane refractive index (n) as well as extinction coefficient (k) of BiOBr measured by spectral ellipsometry [6]. The sample thickness is ~ 1 μm . The measured n and k in telecommunications band are ~ 2.2 and ~ 0.2 , respectively.

3. Z-scan measurement and integration on silicon photonic devices

The third-order optical nonlinear response of the prepared BiOBr nanoflakes was characterized via the open- (OA) and closed-aperture (CA) Z-scan methods [5]. A femtosecond laser source at 800 nm wavelength was used to excite the samples, with a laser pulse duration of ~ 140 fs. Fig. 2(a) and (b) show the representative Z-scan results of the 140-nm BiOBr sample. A typical reverse saturation absorption (RSA) is clearly observed in the OA curve. Since the photo energy (~ 1.55 eV) of the excitation laser is much smaller than the bandgap of BiOBr [7, 8], the observed RSA can be mainly attributed to the TPA of the BiOBr nanoflakes [3, 4]. The peak-valley CA configuration (Fig. 2(b)) indicates the self-defocusing effect in BiOBr nanoflakes, which corresponds to a negative Kerr coefficient n_2 . The measured TPA coefficient β and Kerr n_2 for BiOBr samples with different thicknesses are plotted in Fig. 2(c) and (d). The measured β and n_2 are in the order of $\sim 10^{-7}$ m/W and $\sim 10^{-14}$ m²/W, respectively. In addition, a clear thickness dependence of nonlinear parameters can be observed, where the absolute values of β and n_2 increase with decreasing BiOBr thickness, demonstrating the layer-tunable optical nonlinearity in BiOBr.

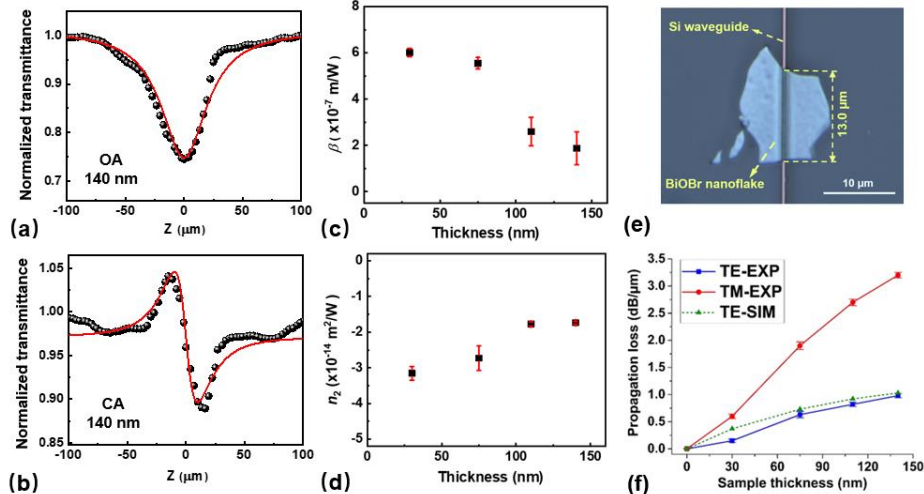


Fig. 2 (a) OA and (b) CA curves of 140-nm BiOBr nanoflake at 800 nm. Measured (c) TPA β and (d) n_2 of BiOBr nanoflakes with different thicknesses. (e) Microscope image of a silicon integrated waveguides incorporated with BiOBr nanoflake. (f) Measured and simulated waveguide propagation losses of the hybrid waveguides for different BiOBr thicknesses.

We also characterize the BiOBr nanoflakes integrated in 220-nm-thick silicon-on-insulator (SOI) waveguides on a 2- μ m-thick buried oxide (BOX) layer. An all-dry transfer method was used to transfer BiOBr nanoflakes onto the silicon integrated waveguides. Fig. 2(e) shows a representative microscope image of a silicon integrated waveguide incorporated with BiOBr nanoflake (~ 110 nm). The width of the waveguide was ~ 500 nm. The BiOBr nanoflake is attached to the silicon integrated waveguide, with an overlap length of ~ 13 μ m. Fig. 2(f) plots the TE and TM polarized waveguide propagation losses of the hybrid integrated waveguides with different BiOBr flake thicknesses. It can be seen that the propagation loss of the hybrid waveguides increases with increasing BiOBr flake thickness, while the TM polarization loss is much higher than TE. We also perform mode analysis for the hybrid integrated waveguides using Lumerical FDTD commercial mode solving software. The experimental and simulated waveguide linear propagation loss (Fig. 2(f)) agree well. These results reflect the stability of the prepared BiOBr nanoflakes and confirm their strong potential as a promising nonlinear optical material for high-performance hybrid integrated photonic devices [10-12]. Finally, as for Si-Ge heterostructures, [13] PdSe₂ may also offer interesting possibilities for 2nd order nonlinear effects courtesy of its complex anisotropic nonlinear optical characteristics.

4. References

- [1] G.-K. Lim *et al.*, "Giant broadband nonlinear optical absorption in dispersed graphene single sheets," *Nat. Photon.* **5**(9), 554–560 (2011).
- [2] G. Demetriou *et al.*, "Nonlinear optical properties of multilayer graphene in the infrared," *Opt. Exp.* **24**(12), 13033–13043 (2016).
- [3] N. Dong *et al.*, "Dispersion of nonlinear refractive index in layered WS₂ and WSe₂ semiconductor films induced by two photon absorption," *Opt. Lett.* **41**(17), 3936–3939 (2016).
- [4] X. Zheng *et al.*, "Characterization of nonlinear properties of black phosphorus nanoplatelets with femtosecond pulsed Z-scan measurements," *Opt. Lett.* **40**(15), 3480–3483 (2015).
- [5] L. Jia *et al.*, "Highly nonlinear BiOBr nanoflakes for hybrid integrated photonics," *APL Photon.* **4**(9), 090802 (2019).
- [6] Y. Yang *et al.*, "Enhanced four-wave mixing in waveguides integrated with graphene oxide," *APL Photon.* **3**(12), 120803 (2018).
- [7] H. Feng *et al.*, "Construction of 2D lateral pseudoheterostructures by strain engineering," *2D Mater.* **4**(2), 025102 (2017).
- [8] J. Di *et al.*, "Bismuth oxyhalide layered materials for energy and environmental applications," *Nano Energy* **41**, 172–192 (2017).
- [9] H. Li *et al.*, "Facet-dependent nonlinear optical properties of bismuth oxychloride single-crystal nanosheets," *J. Mater. Chem. C.* **6**(32), 8709–8716 (2018).
- [10] D. J. Moss *et al.*, "New CMOS-compatible platforms based on SiN and Hydex for nonlinear optics," *Nat. Photon.* **7**(8), 597–607 (2013).
- [11] J. Wu *et al.*, "Graphene Oxide Waveguide and Micro-Ring Resonator Polarizers," *Laser Photonics Rev.* **13**(9), 1900056 (2019).
- [12] J. Wu *et al.*, "Enhanced nonlinear FWM in MRRs integrated with layered GO films," *Small* **16**(16), 1906563 (2020).
- [13] E. Ghahramani, D.J. Moss, and J.E. Sipe, "Large 2nd order nonlinear optical response of strained odd period Si/Ge superlattices on (001) Si substrates," *Physical Review Letters*, **64** (23) pp.2815-2818 (1990). DOI:10.1103/PhysRevLett.64.2815.